Progress In Electromagnetics Research M, Vol. 24, 193–207, 2012

OPTICAL CHARACTERIZATION OF 50 HZ ATMOSPHERIC PRESSURE SINGLE DIELECTRIC BARRIER DISCHARGE PLASMA

M. Y. Naz[1,*], A. Ghaffar[1], N. U. Rehman[2], S. Shukrullah[1], and M. A. Ali[3]

[1]Department of Physics, University of Agriculture Faisalabad, Pakistan

[2]Department of Physics, COMSATS Institute of Information Technology, Islamabad, Pakistan

[3]Department of Physics, Quaid-i-Azam University, Islamabad 45320, Pakistan

Abstract—A low frequency (50 Hz) dielectric barrier discharge (DBD) system with a single dielectric cover on copper coil anode is designed to generate and sustain the micro-discharge plasma which is very practical for material processing applications. The DBD system is powered by a high tension ac source consisting of a conventional step up transformer and variac. The dielectric barriers (quartz and glass) between the conducting electrodes appreciably influences the discharge plasma characterized by optical emission spectroscopy technique. Using intensity ratio method, the electron temperature and electron number density are determined from recorded spectra as function of ac input voltage, type and thickness of dielectric barrier and inter-electrode gap. It is observed that both the electron temperature and electron number density increase with the increase in ac input voltage and ε_r/d ratio, while a decreasing trend is observed with increase in inter-electrode gap.

1. INTRODUCTION

Among the various methods used for the generation of atmospheric pressure micro-discharge plasmas, the dielectric barrier discharge (DBD) method is always favored because of its simple and flexible

Received 24 January 2012, Accepted 23 March 2012, Scheduled 1 May 2012

* Corresponding author: Muhammad Yasin Naz (yasin603@yahoo.com).

geometry. The DBDs also referred as silent discharges are predestined for discharge applications of plasma chemistry at large volumes. The main feature of DBDs is to establish the non-equilibrium discharge conditions at atmospheric pressure in an economic and reliable way [1]. This feature of DBDs is of great importance in material processing, sterilization, pollution control, surface activation, chemical vapor deposition, ultraviolet or vacuum ultraviolet excimer lamps, bio-treatment of micro-organisms and aerodynamical flow control.

Most of DBDs can successfully be operated with high frequencies ranging from few kHz to few MHz [2, 3]. These high frequency operations are necessary for production of metastable species which play a major role during the generation of discharge plasmas through penning ionization. But the most important drawback of high frequency DBDs is the requirement of very complicated impedance matching networks and excessive power losses via dielectric barrier heating [4, 5]. On the other hand, the low frequency DBDs ranging from few Hz to few kHz require very simple or no impedance matching network which makes these systems more practical for industrial applications. By considering this feature of low frequency operations, a conventional step up transformer with 50 Hz ac input can be used to generate and sustain atmospheric pressure DBDs [6].

The DBD characteristics can mainly be controlled by the ac input voltage, input frequency, inter-electrode gap, nature of dielectric material, temperature, moisture, working gas pressure and gas flow rate. Therefore, the successful generation and characterization of DBDs require at least one dielectric barrier to be placed between the ac powered cylindrical or planar conducting electrodes. In most common configurations DBDs have dielectric cover on both electrodes but the DBD geometry with single dielectric barrier does not allow the charges to accumulate on the electrode surface and all the charge to move into the electrical system. The typical materials like glass, quartz, ceramics, alumina and polymers with low dielectric loss and relatively high breakdown strength can serve this purpose [7].

The thermal, optical and electrical properties of DBDs are mainly dependent on the permittivity and the thickness of dielectric barrier [8]. The ratio of relative permittivity and thickness ($\varepsilon_r/_d$) determines the amount of the charge transferred in the gas discharge and has significant impact on electron number density and the density of reactive species [9]. The electronic equivalent circuit of DBD system with single dielectric barrier between the conducting electrodes is shown in Fig. 1 [7]. In this figure, $V_\circ$ is the ac input voltage, $I_\circ$ is the total current in the circuit, C_g is the capacitance of the inter-electrode gas gap and C_d is the capacitance of the dielectric barrier which can

be determined using the equation:

$$C_d = \frac{\varepsilon_r \varepsilon_o A}{d} \tag{1}$$

FromEquation (1) and $Q = C_d V$, the electron temperature and electron number density can be enhanced easily by using the dielectric barriers of higher relative permittivities and relatively small thickness.

The optical emission spectroscopy (OES) is one of the most popular tools to characterize the discharge plasmas. It is very simple in its implementation and provides detailed information about plasma parameters such as electron temperature (kT_e), electron number density (n_e), electron energy distribution function (EEDF) [10], densities of excited species, ionization and dissociation of discharge plasma species [11]. During the chemical reactions and excitation processes associated with reactive species, the electron impact causes a small fraction of discharge plasma species to move into upper excited states. These excited states decay and emit characteristic radiations in the visible and near ultraviolet range. It shows that kT_e is of great importance during the production of plasma active species through inelastic collisions of electrons with working gas molecules [8, 11].

The present work includes the spectroscopic characterization of atmospheric pressure air DBD with single dielectric barrier between the conducting electrodes. The atmospheric pressure discharge was generated and sustained using conventional step up transformer at different excitation ac voltages while keeping the input frequency fixed at 50 Hz throughout. The kT_e and n_e were determined as function of excitation voltages and inter electrode gaps. Moreover, the dielectric barriers (quartz, glass) having different relative permittivities and ε_r/d ratios were used and their influence on kT_e and n_e was also studied. The ultimate aim of the present research work is to get control over discharge plasma parameters such as kT_e and n_e for the optimum conditions of discharge plasmas to be used for material processing applications.

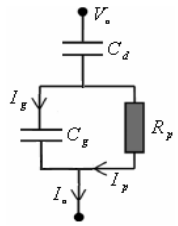

Figure 1. Electrical equivalent circuit of a DBD system with single dielectric barrier.

2. EXPERIMENT SETUP

The schematic diagram of experimental setup used for generation and characterization of low frequency atmospheric pressure air DBD is shown in Fig. 2. It consists of an ac grounded aluminum electrode (11 cm × 5 cm × 2 cm) with an active surface area of 55 cm^2 and a copper coil anode (1.2 mm in diameter) having 30 turns in total [12, 13]. Two kinds of dielectric barriers; quartz and glass are used separately for DBD generation. Each of the dielectric barriers has its own specific relative permittivity as listed in Table 1. The diameter of the anode is made of good fit inside the quartz and class tubes of inner diameter 15 mm each. The spacing between the dielectric barrier and the grounded electrode is kept constant at 1, 1.2, 1.4 and 1.6 mm.

The dielectric barrier cover on copper coil anode is the key for proper functioning of the DBDs. In the absence of the dielectric barrier, the DBD undergoes to an arc transition region. The thickness of the dielectric barrier cover is also kept very small which allows maximum power to pass through the dielectric barrier to cause electrical breakdown of the working gas at atmospheric pressure. But in the presence of dielectric barrier on one of the conducting electrodes, the DBDs can not be generated through a dc source. Therefore, a high tension ac source comprising of a step up transformer and a variac is used to generate and sustain the atmospheric pressure DBD at 10, 11, 12, 13, 14 and 15 kV. The step up transformer may provide up to 50 kV at the output terminals with ac current of 200 mA. For its peak output, the primary of the step up transformer consumes 250 V at 50 Hz frequency with ac current of 45 A. The turn's ratio of primary to secondary winding of this step up transformer is 1 : 200. The

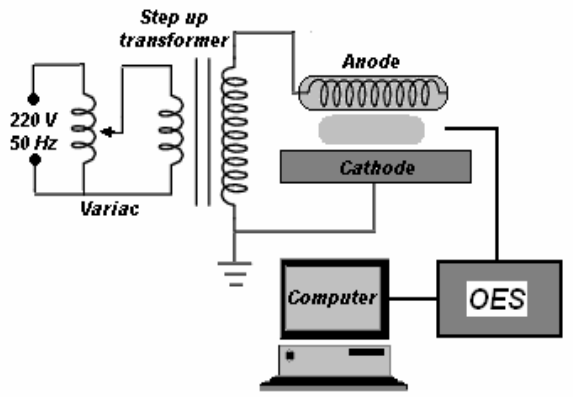

Figure 2. Schematic diagram of experimental setup.

Table 1. Main features of tested dielectric barriers.

Material	Barrier thickness (mm)	Relative permittivity (ε_r)	ε_r/d ($^1/_{mm}$)
Quartz	1.0	4.22	4.220
	1.5		2.813
	1.8		2.344
Glass	1.0	8.63	8.630
	1.5		5.753
	1.8		4.794

variac varies the ac voltage at the input of the step up transformer which makes plausible to obtain the desired ac voltage at the output terminals. The digital multimeters are used to monitor the voltage and current in the DBD circuit.

For the determination of kT_e and n_e, the DBD induced spectroscopy is carried out using a computer controlled system consisting of an Ocean Optic Spectrometer (HR: 4000 CG UV-NIR) and an optical fiber. This spectrometer has optical resolution of 0.025 nm and wavelength range of 200 nm to 1100 nm. Having the integration time of 4 ms to 20 s this spectrometer can perform full scan into memory after every 4 ms with the USB 2.0 and after every 600 ms with the serial port. The light signal from optical fiber is focused onto the slit of the spectrometer via collimated lens where it is collected by the detector of the spectrometer. The detector is a light sensitive semiconductor chip which converts the light signal into an electrical signal. The spectrometer transmits this electrical signal to the computer and the resultant spectra is recorded in the range of 300 nm to 600 nm as function of input voltage, type and thickness of dielectric barrier and inter-electrode gap to investigate the influence of discharge plasma parameters on the spectral intensities of the selected emission bands and lines.

3. EXPERIMENTAL RESULTS AND DISCUSSION

3.1. Optical Emission Spectroscopy

In this experiment, air was used as a working gas for DBD generation. It consists of nitrogen (78.08%), oxygen (20.95%), carbon dioxide (0.038%), argon (0.93%) and small traces of other gases. The used air also contains around 1% of water vapors. Due to atmospheric pressure and a blend mixture of gases, there is a series of chemical

recombinations which can cause the extinction of discharge and large amount of energy (several keV) is required to sustain the atmospheric pressure DBDs. When the ac input voltage reaches to certain breakdown value, the plasma discharge begins with some filamentary distributions on dielectric barrier surface and become consistent with the increase of applied voltage. In DBDs, the electrons gain energy from the applied ac electric field and transfer it to the neutral plasma species through inelastic collisions. These inelastic collisions excite some of the plasma species into the higher energy states which decay back to lower energy states by emitting the photons of characteristic wavelengths. The intensities of these spectral lines can be used for determinations of kT_e and n_e. The spectroscopic technique used to determine kT_e is based on the measurement of the relative intensities of two or four spectral lines of same atomic species [14]. The emission line intensity of these spectral lines is kT_e dependent and always proportional to the population density of excited states. So kT_e can be determined from the emission spectrum using the well-know Boltzmann plot:

$$kT_e = (E_2 - E_1)\left[\ln \frac{I_1 \lambda_1 g_2 A_2}{I_2 \lambda_2 g_1 A_1}\right]^{-1} \tag{2}$$

In this equation, indices 1 and 2 refer to the first and second spectral lines; I represents the measured intensity of the selected spectral lines; k is the Boltzman constant; E is the excited state's energy; g is the statistical weight; A is the transition probability. The Boltzmann plot

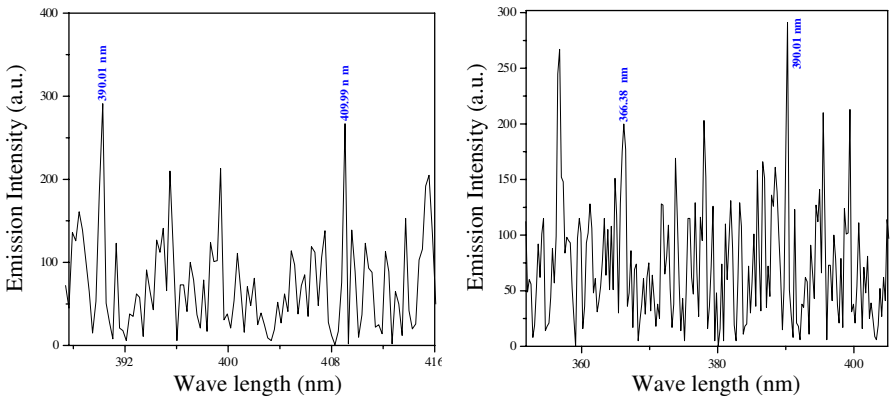

Figure 3. Emission spectrum used for determination of electron temperature at ac input voltage of 10 kV and inter-electrode gap of 1 mm.

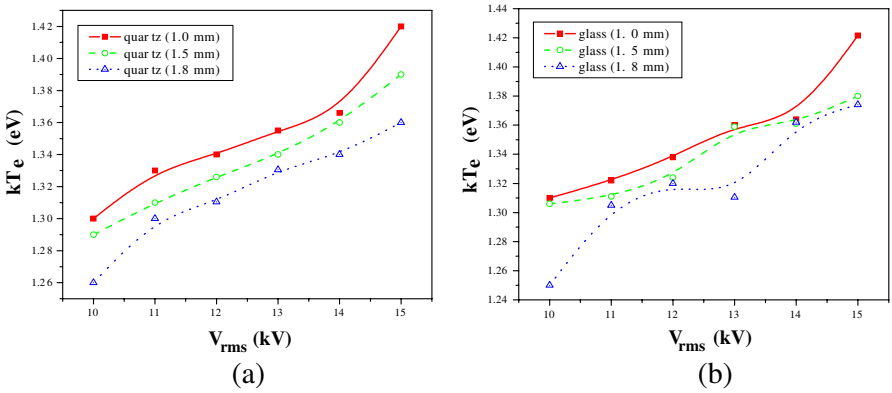

Figure 4. (a) Electron temperature versus ac input voltage with quartz dielectric barrier. (b) Electron temperature versus ac input voltage with glass dielectric barrier.

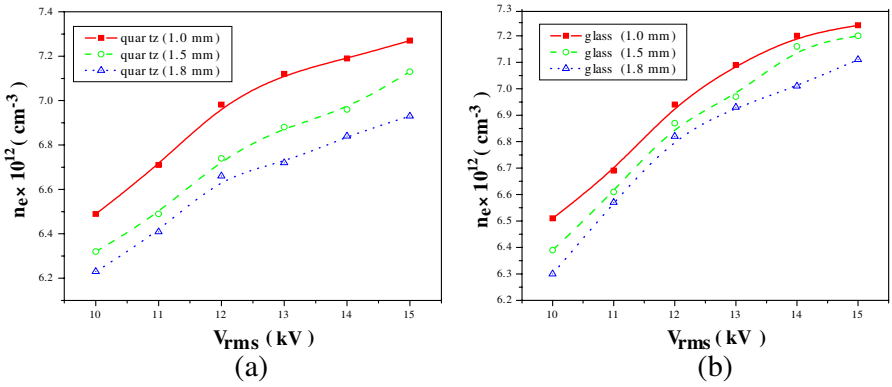

Figure 5. (a) Electron number density versus ac input voltage with quartz dielectric barrier. (b) Electron number density versus ac input voltage with glass dielectric barrier.

method is only valid if the discharge plasma under study is in complete local thermodynamic equilibrium (LTE). But in our experiment, it is difficult that this condition will hold due to low plasma density. Therefore, in the present atmospheric pressure DBD, this method may not be used for the exact determination of kT_e and n_e. Nevertheless, it can provide us estimated values of these plasma parameters under varying working conditions of discharge plasma [11]. A typical atmospheric pressure DBD spectrum for single quartz dielectric barrier (1 mm) and 1 mm inter-electrode gap at 10 kV ac input is shown in Fig. 3(a). The spectrum was recorded, nitrogen and oxygen emitted

lines were observed in the range of 300 nm to 600 nm. Then kT_e was determined by selecting two N-I lines of observed spectrum. These lines result from the transition of $^3P_{3/2}$ state to $^3S_{1/2}$ state at 409.99 nm and $^5P_{3/2}$ state to $^3S_{3/2}$ state at 390.01 nm. The intensity of N-I spectral lines was obtained from the spectrum by integrating over line profile and normalizing with the spectral response of the instrument [15]. The E, g and A for selected lines can be taken from the NIST Atomic Spectra Datasheet [16]. Putting all these values in Equation (2), we can obtain kT_e as function of applied ac voltage, inter-electrode gap and dielectric barrier thickness as shown in Fig. 4. Finally, the Boltzman and Saha equations were used to determine the n_e from the relative intensities of atomic and ionic spectral lines [16, 17].

$$n_e = \left[(2\pi mkT_e)^{3/2}/h^3\right]\left[2A^+g^+\lambda^0 I^0/A^0g^0\lambda^+ I^+\right] \exp\left[-\left(E^+ - E^0 + E_i^0 - \Delta E_i\right)/kT_e\right] \quad (3)$$

In this equation, (0, +) denote the neutral and ionized atoms; kT_e is the electron temperature; E is the energy of the emissive levels; E_i^0 is ionization energy of neutral atoms; ΔE_i is the lowering of ionization energy. The N-I and N-II lines used for the determination of n_e are identified and labeled in Fig. 3(b). These lines result from the atomic transition of $^5P_{3/2}$ state to $^3S_{3/2}$ state at 390.01 nm and ionic transition of $4S$ state to $3P$ state at 366.38 nm. By comparing the intensities of these spectral lines we can determined n_e as function of ac applied voltage, inter-electrode gap and dielectric barrier thickness as shown in Fig. 5.

3.2. Excitation and Dissociation Reactions

The OES can reliably be employed to monitor the discharge plasma states. However, the use of OES for the determination of average energy of free electrons in discharge plasmas requires careful analysis of the kinetic process involved in population and depopulation of the excited states of discharge plasma species. In atmospheric pressure DBDs with air as a working gas, the highly energetic electrons play key role during the excitation and ionization of corresponding oxygen and nitrogen bands. Some of the important chemical reactions induced by these energetic electrons are as follow:

$$e + N_2\left(X^1\sum_g^+\right)\upsilon = 0 \longrightarrow N_2\left(C^3\Pi_u\right)\upsilon' = 0 + e$$

where, $N_2(C^3\Pi_u)$ state of nitrogen can be populated by the number of excitation and quenching processes. These processes involve electron

impact excitation (from ground state $N_2(X^1\sum_g^+)$ and first metastable state $N_2(A^3\sum_u^+)$), pooling reactions, associative excitation, energy transfer between colliding particles and penning excitation [11]. The radiative decay of subsequent states emit the characteristic photons of (0-0) band of second positive system at 337.1 nm which is identified in the recorded spectrum [14].

$$N_2\left(C^3\Pi_u\right)\upsilon' \rightarrow N_2\left(B^3\Pi_g\right)\upsilon' = o + h\upsilon$$

Similarly, the direct impact ionization from the ground state $N_2(X^1\sum_g^+)$ populates the $N_2^+(B^2\sum_u^+)$ excited state [14].

$$e + N_2\left(X^1\sum_g^+\right) \rightarrow N_2^+\left(B^2\sum_u^+\right) + 2e$$

Again the $N_2^+(B^2\sum_u^+)$ excited state emits the characteristic photons of (0-0) band of first negative system as identified in recorded spectrum [11, 14]. The emission intensity of the band is proportional to the population density of the $N_2^+(B^2\sum_u^+)\upsilon' = 0$ state.

$$N_2^+\left(B^2\sum_u^+\right)\upsilon' = 0 \rightarrow N_2^+\left(X^2\sum_g^+\right)\upsilon = o + h\upsilon$$

In atmospheric pressure DBDs, the degree of dissociation due to direct electron impact on nitrogen molecules is also an important discharge plasma parameter. It plays very vital role in material processing applications. The following chemical kinetics is involved in the dissociation of nitrogen molecules.

$$e + N_2\left(X^1\sum_g^+, \nu = 0\right) \rightarrow e + N\left(^4S\right) + N\left(^4S\right)$$

$$e + N_2\left(X^1\sum_g^+, \nu = 0\right) \rightarrow e + N\left(^4S\right) + N\left(^2D\right)$$

The dissociation of nitrogen molecules results into the production of N radicals which have very high concentration and chemical reactivity at atmospheric pressure. This property of atomic nitrogen is of significant importance in industrial applications of DBDs. Apart from this, the dissociation of oxygen molecules and production of atomic oxygen with high chemical reactivity also play very important role in surface oxidation applications which result into the improvement of wettability and adhesive properties of treated surfaces.

3.3. Discussion

The graphical representations of the results obtained for kT_e and n_e as function of ac input voltage and different constant values of dielectric barrier thickness (1, 1.5, 1.8 mm) are shown in Figs. 4 and 5. In DBD plasmas, the kT_e not only controls the production rate of active species through inelastic collisions but also helps to determine the rate process of plasma reactive gases. Therefore, it is important to regulate kT_e to get good control over selected processes occurring in DBD plasmas. From Fig. 4, it is observed that kT_e increases with increase of ac input voltage. [18]. This increasing trend in kT_e under the influence of rising ac input voltage might be due to the increase in kinetic energy of the discharge plasma electrons. But the most important reason of this increment is the availability of more and more highly energetic electrons in high energy tail of the electron energy distribution function (EEDF) at relatively higher input voltages [19]. As the relation for mean energy of electrons is:

$$\bar{E} = qE\lambda_e = \frac{qV\lambda_e}{X} = \frac{q\pi r_i^2}{Xk_BT}\left(\frac{V_{\text{rms}}}{P}\right) \tag{4}$$

where, V is the ac input voltage, X the inter-electrode gap, E the electric field strength, λ_e the mean free path, r_i the ionic radius, and k_B the Boltzmann constant. Equation (4) shows that at constant filling gas pressure (atmospheric pressure), the mean free path of the electrons also remains constant but if we increase the ac input voltage then the availability of the highly energetic electrons capable of ionization also increases and consequently the kT_e. This increment in excitation and ionization events with ac input voltage also has proportional effect on n_e. Furthermore, the low frequency DBDs consist of many microdischarges. The number of these microdischrges increases with the increase in ac input voltage which indirectly indicates a rise in n_e. Apart from these, it is also clear from Equation (3) that n_e has direct relation with kT_e. It means if kT_e increases, the n_e will also increase as observed in this experiment.

Beside the applied ac input voltage, the thickness and type of dielectric barrier also have significant effect on discharge plasma parameters [20]. Figs. 4 and 5 also demonstrate the dependence of kT_e and n_e on the thickness of the dielectric barrier used. The results were obtained with quartz and glass dielectric barrier having thickness of 1, 1.5 and 1.8 mm. From these results, it can be observed that both kT_e and n_e increase with the decrease in thickness of the dielectric barrier. It means thinner the dielectric barrier, higher will be the ε_r/d ratio and excess of the charge transfer will take place. Hence, even at same ac input voltages, the electron temperature and density of the excited

states will be enhanced due to higher ε_r/d ratio. However, the thinner dielectric barriers could also have a negative impact on DBDs that is the electrical breakdown can occur if the thickness of the dielectric barrier is too short [7]. It is also observed that for thinner dielectric barriers (1 mm), the n_e and kT_e in particular become independent of dielectric barrier material as shown in Fig. 6. Although the ε_r of glass is much higher than the quartz but values of discharge plasma parameters obtained with quartz dielectric barrier are comparable to that obtained with glass dielectric barrier at smaller barrier thicknesses (1 mm). It might be due to the higher secondary electron emissions coefficient of the quartz which plays a dominant role in DBDs generated with thinner dielectric barriers.

The electrical breakdown problem can be overcome by using the dielectric barriers with higher relative permittivities rather than very small thicknesses. It will permit very high values of the charge to be transferred without occurrence of electrical breakdown. The results in Figs. 4 and 5 also show that the kT_e and n_e obtained with glass dielectric barrier ($\varepsilon_r = 8.63$) are higher than those obtained with quartz ($\varepsilon_r = 4.22$) dielectric barrier of same thickness. It means the efficiency of DBDs can be enhanced by using dielectric barriers with higher values of ε_r [7, 21].

Finally, the effect of inter-electrode gap on discharge plasma parameters was also investigated, and a decreasing trend was observed in kT_e and n_e with increase in inter-electrode gap. Fig. 7 gives the graphical representation of the plasma parameters as functions of the inter-electrode gap. Using the relation $V = Q/C$ and Equation (1), we

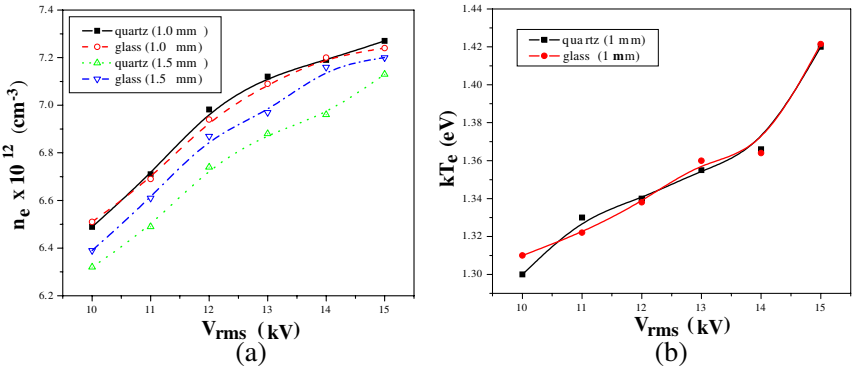

Figure 6. (a) Comparison of electron number density for quartz and glass dielectric barriers. (b) Comparison of electron temperature for quartz and glass dielectric barriers.

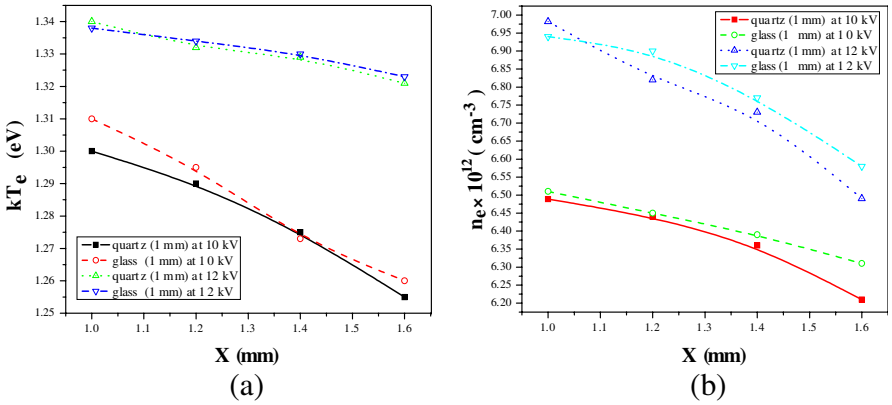

Figure 7. (a) Electron temperature versus inter-electrode gap. (b) Electron number density versus inter-electrode gap.

can justify the observed behavior of the plasma parameters at different values of inter-electrode gap [7, 11, 14]. Many authors have researched on plasma study [22–24].

4. CONCLUSIONS

An atmospheric pressure DBD system with single dielectric barrier between the conducting electrodes is designed to generate low frequency (50 Hz) micro-discharge plasma which is very practical for material processing applications. The single dielectric barrier between the electrodes appreciably influences the discharge plasma, characterized by optical emission spectroscopy technique. The electron temperature and electron number density are determined as function of ac input voltage, type and thickness of dielectric barrier material and inter-electrode gap.

It is found that the electron temperature and electron number density increase with the increase in ac input voltage but decrease with the increase in inter-electrode gap. The choice of an appropriate dielectric barrier material and its thickness can also improve the efficiency of DBDs significantly. As different dielectric materials have different relative permittivity and consequently the $\varepsilon_r/_d$ ratio. However, the higher values of $\varepsilon_r/_d$ ratio can cause additional effects. All the materials with significant relative permittivity may not have adequate dielectric barrier strength which can result into the electrical breakdown. So it will be advantageous to use the materials with higher secondary electron emission coefficient especially in case of thin

dielectric barriers. Finally, the electron temperature and electron number density measured in atmospheric pressure DBD are found to have significant values for generation of reactive species (atomic nitrogen and oxygen) to be used for surface modifications.

ACKNOWLEDGMENT

The work was partially supported by the Higher Education Commission (HEC) via Research Project No. 20-1789/R&D for low temperature plasma physics.

REFERENCES

1. Kostov, K. G., R. Y. Honda, L. M. S. Alves, and M. E. Kayama, "Characterization of dielectric barrier discharge reactor for material treatment," *Brazilian Journal of Physics*, Vol. 39, No. 2, 2009.
2. Pandey, R. S. and D. K. Singh, "Study of electromagnetic ion-cyclotron instability in a magnetoplasma," *Progress In Electromagnetics Research M*, Vol. 14, 147–161, 2010.
3. Pandey, R. S., "Cold plasma injection on VLF wave mode for relativistic magnetoplasma with A.C. Electric Field," *Progress In Electromagnetics Research C*, Vol. 2, 217–232, 2008.
4. Yongh, K., M. S. Cha, W. H. Shin, and Y. H. Song, "Characterization of dielectric barrier glow discharges with a low frequency generator in nitrogen," *Journal of the Korean Physical Society*, Vol. 43, No. 5, 2003.
5. Shi, L., B. L. Guo, Y. M. Liu, and J. T. Li, "Characterization of plasma sheath channel and its effect on communication," *Progress In Electromagnetics Research*, Vol. 123, 321–336, 2012.
6. Osawa, N. and Y. Yoshioka, "Generation of low-frequency homogeneous dielectric barrier discharge at atmospheric pressure," *IEEE Transactions on Plasma Science*, Vol. 40, No. 1, 2011.
7. Meiners, A., M. Leck, and B. Adel, "Efficiency enhancement of a dielectric barrier plasma discharge by dielectric barrier optimization," *Review of Science Instruments*, Vol. 81, 113507, 2010.
8. Anghel, S. D., "Generation and electrical diagnostic of an atmospheric-pressure dielectric barrier discharge," *IEEE Transactions on Plasma Science*, Vol. 39, No. 3, 2011.
9. Kogelschatz, U., "Atmospheric-pressure plasma technology," *Plasma Physics and Controlled Fusion*, Vol. 46, No. B63, 2004.

10. Jain, R. and M. V. Kartikeyan, "Design of a 60 GHz, 100 kW CW gyrotron for plasma diagnostics: GDS-V.01 simulations," *Progress In Electromagnetics Research B*, Vol. 22, 379–399, 2010.
11. Khan, F. U., N. U. Rehman, S. Naseer, M. A. Naveed, A. Qayyum, N. A. D. Khattak, and M. Zakaullah, "Diagnostic of 13.56 MHz RF sustained Ar-N_2 plasma by optical emission spectroscopy," *Eur. Physic, J. Appl. Phys.*, Vol. 45, 11002, 2009.
12. Costa, E. M. M., "Parasitic capacitances on planar coil," *Journal of Electromagnetic Waves and Applications*, Vol. 23, Nos. 17–18, 2339–2350, 2009.
13. Shiri, A. and A. Shoulaie, "A new methodology for magnetic force calculations between planar spiral coils," *Progress In Electromagnetics Research*, Vol. 95, 39–57, 2009.
14. Chapelle, P., T. Czerwiec, and J. P. Bellot, "Plasma diagnostic by emission spectroscopy during vacuum arc remelting," *Plasma Source Sci. Technol.*, Vol. 11, 303–304, 2002.
15. Jandieri, G. V., A. Ishimaru, V. Jandieri, and N. N. Zhukova, "Depolarization of metric radio signals and the spatial spectrum of scattered radiation by magnetized turbulent plasma slab," *Progress In Electromagnetics Research*, Vol. 112, 63–75, 2011.
16. Fozza, A. C., M. Moisan, and M. R. Wertheimer, "Vacuum ultraviolet to visible emission from hydrogen plasma: Effect of excitation frequency," *J. Appl. Phys.*, Vol. 88, No. 20, 2000.
17. Heald, M. A. and C. B. Waharton, *Plasma Diagnostics with Microwaves*, John Wiley & Sons Inc., New York, 1978.
18. Naz, M. Y., A. Ghaffar, N. U. Rehman, M. Azam, S. Shukrullah, A. Qayyum, and M. Zakaullah, "Symmetric and asymmetric double langmuir probes characterization of radio frequency inductively coupled nitrogen plasma," *Progress In Electromagnetics Research*, Vol. 115, 207–221, 2011.
19. Naz, M. Y., A. Ghaffar, N. U. Rehman, S. Naseer, and M. Zakaullah, "Double and triple Langmuir probes measurements in inductively coupled nitrogen plasma," *Progress In Electromagnetics Research*, Vol. 114, Nos. 113–128, 2011.
20. Ai, X., Y. Han, C. Y. Li, and X. W. Shi, "Analysis of dispersion relation of piecewise linear recursive convolution FDTD method for space-varying plasma," *Progress In Electromagnetics Research Letters*, Vol. 22, 83–93, 2011.
21. Gurel, C. S. and E. Oncu, "Interaction of electromagnetic wave and plasma slab with partially linear and sinusoidal electron density profile," *Progress In Electromagnetics Research Letters*,

Vol. 12, 171–181, 2009.

22. Pavelyev, A. G., Y.-A. Liou, J. Wickert, K. Zhang, C.-S. Wang, and Y. Kuleshov, "Analytical model of electromagnetic waves propagation and location of inclined plasma layers using occultation data," *Progress In Electromagnetics Research*, Vol. 106, 177–202, 2010.
23. Qian, Z. H., R.-S. Chen, K. W. Leung, and H. W. Yang, "FDTD analysis of microstrip patch antenna covered by plasma sheath," *Progress In Electromagnetics Research*, Vol. 52, 173–183, 2005.
24. Sternberg, N. and A. I. Smolyakov, "Resonant transparency of a three-layer Structure containing the dense plasma region," *Progress In Electromagnetics Research*, Vol. 99, 37–52, 2009.